Supplementary Data

Robust, tunable genetic memory from protein sequestration combined with positive feedback

Tatenda Shopera, William R. Henson, Andrew Ng, Young Je Lee, Kenneth Ng and Tae Seok Moon

Table of Contents

List of Figures

List of Tables

1. Modeling the ExsADC system

To determine the response of each constructed circuit, we made the following assumptions:

1. The protein-protein interactions between ExsA, ExsD, and ExsC occur on a much faster timescale than transcription, translation, and protein degradation/dilution.
2. At the time of measurement, our system is at steady state.

To describe the interactions between ExsA, ExsD, and ExsC, we used a combination of mass balance equations and ordinary differential equations. We can define the mass balances for each protein as

$$A_0 = A + AD, \tag{1}$$

$$D_0 = D + AD + DC, \text{ and} \tag{2}$$

$$C_0 = C + DC. \tag{3}$$

Here A_0, D_0, and C_0 are the total protein concentrations of ExsA, ExsD, and ExsC, respectively. A, D, and C are the concentrations of unbound ExsA, ExsD, and ExsC, respectively. AD is the concentration of the ExsA-ExsD protein complex and DC is the concentration of the ExsD-ExsC protein complex. The stoichiometry for the ExsA-ExsD interaction[1] as well as the ExsD-ExsC interaction[2] has been reported to be 1:1.

Next, we used ordinary differential equations (ODEs) to describe production and degradation of each protein over time. The ODEs describing the changes of the total protein concentration A_0, D_0, C_0, and green fluorescent protein (gfp) can be written as[3]

$$\frac{dA_0}{dt} = \alpha_A \beta_A pBAD - \gamma_A A_0, \tag{4}$$

$$\frac{dD_0}{dt} = \alpha_D \beta_D pTet^* - \gamma_D D_0, \tag{5}$$

$$\frac{dC_0}{dt} = \alpha_C \beta_C pLux^* - \gamma_C C_0, \tag{6}$$

And

$$\frac{dgfp}{dt} = \alpha_{gfp} \beta_{gfp} pexsD - \gamma_{gfp} gfp. \tag{7}$$

Here α_A, α_D, α_C, and α_{gfp} are the transcription rates for the respective promoters. β_A, β_D, β_C, and β_{gfp} are the translation rates for each protein. *pBAD*, *pTet**, *pLux**, and *pexsD* are the promoter activities for each promoter (as defined below). γ_A, γ_D, γ_C, and γ_{gfp} are the degradation/dilution rates for each protein. At steady state,

$$A_0 = \frac{\alpha_A \beta_A}{\gamma_A} pBAD = \theta_A{}' pBAD, \tag{8}$$

$$D_0 = \frac{\alpha_D \beta_D}{\gamma_D} pTet^* = \theta_D{}' pTet^*, \tag{9}$$

$$C_0 = \frac{\alpha_C \beta_C}{\gamma_C} pLux^* = \theta_C{}' pLux^*, \tag{10}$$

And

$$gfp = \frac{\alpha_{gfp} \beta_{gfp}}{\gamma_{gfp}} pexsD = \theta_{gfp}{}' pexsD. \tag{11}$$

The terms $\theta_A{}'$, $\theta_D{}'$, $\theta_C{}'$, and $\theta_{gfp}{}'$ represent scaling factors that account for changes in gene expression and protein degradation due to various factors, including gene copy numbers, ribosome binding site (RBS) strength, and culture conditions affecting growth/dilution rates.

We also used relationships between the concentrations of the free regulators and the complexes (ExsA-ExsD and ExsD-ExsC) at steady state. The dissociation constants can be defined as

$$K_{AD} = \frac{A \cdot D}{AD} \tag{12}$$

And

$$K_{DC} = \frac{D \cdot C}{DC}, \tag{13}$$

The above mass balances, ODEs, and dissociation constant equations form the foundation for the modeling of each circuit constructed in this study.

2. Transfer functions of the two- and three-member systems (Fig. 1b and 1c)

Two-member system

For the two-member system shown in Fig. 1b, the solution for the free ExsA concentration can be obtained from Equations 1, 2, and 12 (which lead to a quadratic equation with $DC = 0$) and is[4,5]

$$\begin{aligned} A &= \frac{1}{2}\left[(A_0 - K_{AD} - D_0) + \sqrt{(A_0 - K_{AD} - D_0)^2 + 4K_{AD}A_0}\right] \\ &= \frac{1}{2}\left[(A_0 - K_{AD} - D_0) + \sqrt{(A_0 + K_{AD} + D_0)^2 - 4A_0D_0}\right]. \end{aligned} \tag{14}$$

This equation was used in conjunction with the general form of the pexsD transfer function

$$pexsD = F_{max} \frac{A}{A + K_{D,pexsD}} + F_{min} \tag{15}$$

where *pexsD* is the promoter activity of the pexsD promoter, F_{max} is the maximal promoter activity, $K_{D,pexsD}$ is the half-maximal concentration, and F_{min} is the basal promoter activity. The Hill coefficient of the pexsD promoter was set to one, which was based on both the previous report[6] and our analysis of the transfer function (Fig. S2).

The transfer functions for the pBAD, pTet*, and pLux* promoters were described by the general Hill equation:

$$P_x = F_{max}\frac{I^{n_x}}{I^{n_x} + K_x^{n_x}} + F_{min} \tag{16}$$

where P_x is the promoter activity of the promoter x, I is the inducer concentration for each promoter, n_x is the Hill coefficient, and K_x is the half-maximal concentration. The promoter activity of each inducible system (pBAD-*gfp*, pTet*-*gfp*, and pLux*-*gfp*) was characterized independently and was fitted to the model (Equation 16, Table S1). The values of A_0, D_0, and C_0 in Equations 8-10 were described using promoter activities (the promoter activity of pBAD, pTet*, and pLux*, respectively). From Equations 11 and 15, the equation for the circuit output can be written as

$$output = \theta_{gfp}\left(\frac{A}{A + K_{D,pexsD}} + \frac{F_{min}}{F_{max}}\right), \tag{17}$$

where $\theta_{gfp} = \frac{\alpha_{gfp}\beta_{gfp}}{\gamma_{gfp}}F_{max}$. The equation for the free ExsA concentration (Equation 14) was used to calculate the value for A in Equation 17. All protein concentrations were non-dimensionalized by K_{AD} in both the two- and three-member systems. This non-dimensionalization yields the equation

$$output = \theta_{gfp}\left(\frac{\left[\left(\widehat{A_0} - 1 - \widehat{D_0}\right) + \sqrt{\left(\widehat{A_0} + 1 + \widehat{D_0}\right)^2 - 4\widehat{A_0}\widehat{D_0}}\right]}{\left[\left(\widehat{A_0} - 1 - \widehat{D_0}\right) + \sqrt{\left(\widehat{A_0} + 1 + \widehat{D_0}\right)^2 - 4\widehat{A_0}\widehat{D_0}}\right] + \kappa} + \frac{F_{min}}{F_{max}}\right) \tag{18}$$

Here, $\widehat{A_0} = A_0/K_{AD}$, $\widehat{D_0} = D_0/K_{AD}$, and $\kappa = 2K_{D,pexsD}/K_{AD}$.

To generate the model heat map for the two-member system, the raw fluorescence data were fit to the model (Equations 14-18) by using fmincon in MATLAB 2014b. Certain parameters were constrained between upper and lower bounds set from the promoter characterization (Table S1). All values were bounded to ensure that the values for the model were constrained to biologically feasible values. Table S2 lists the final parameter values.

Table S1. Parameters of pBAD, pTet*, and pLux* promoter transfer functions. All data were normalized to the maximum GFP output from each promoter. The ± values represent the 95% confidence interval (CI). Data were fit to the model (Equation 16) and R^2 values for each fit were > 0.95.

Promoter	n	K	F_{min} (a.u.)	F_{max} (a.u.)
pBAD	1.6 ± 0.4	56 ± 8 (μM)	0.001 ± 0.033	0.95 ± 0.06
pTet*	1.8 ± 1.6	370 ± 210 (pg/mL)	-0.05 ± 0.22	0.93 ± 0.20
pLux*	2.6 ± 0.4	4.6 ± 0.3 (nM)	0.002 ± 0.019	0.98 ± 0.03

Three-member system

For the three-member system (Fig. 1c), a new equation for the non-dimensionalized A concentration was derived in a similar manner to Equation 14 by substituting the dissociation constants (Equations 12 and 13) into the mass balance equations (Equations 1-3) and solving for the non-dimensionalized concentration $\hat{A}$. We obtained the equation relating $\hat{A}$ as a function of other parameters, which can be expressed as a 3rd order polynomial

$$a\hat{A}^3 + b\hat{A}^2 + c\hat{A} + d = 0\,. \tag{19}$$

This equation was solved simultaneously with the other non-dimensionalized equations mentioned above, and the value for $\hat{A}$ was substituted into the non-dimensionalized version of Equation 17 to which the experimental data were fitted by using MATLAB 2014b (Table S2).

To determine the accuracy of the models for the two- and three-member systems, the model values and the experimental data were compared (Fig. S1). The expected model outputs correlate well with the experimental data (R^2 > 0.92 for all three cases).

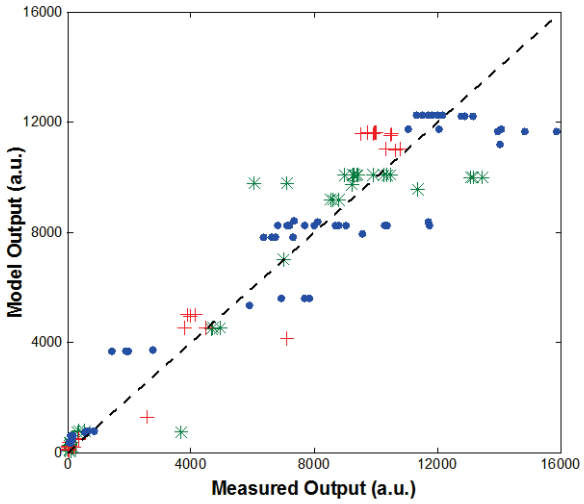

Figure S1. Comparison between the transfer function model and the experimental data (Fig. 1). The dashed line represents the y=x line. Green stars (*), the values from the two-member system (R^2 = 0.95); the red crosses (+), the values from the three-member system with a low C concentration (R^2 = 0.97); and the blue circles (•), the values from the three-member system with a high C concentration (R^2 = 0.92).

Table S2. Parameters for the two- and three-member systems (Fig. 1).

Parameter	Two-member	Three-member	Units
θ_A/K_{AD}	69	0.98	a.u.
θ_D/K_{AD}	780	11	a.u.
κ	5	5	unitless
K_{DC}/K_{AD}	Not Applicable	0.18[+]	unitless
pBAD, n	1.3	2.0	unitless
pBAD, K	47	50	μM
pTet*, n	3.3	3.3	unitless
pTet*, K	241	160	pg/mL
θ_{gfp}	0.80	4.6	a.u.
pexsD F_{min}/F_{max}	0.002	0.002	unitless
pBAD F_{min}/F_{max}	0.009	0.009	unitless
pTet* F_{min}/F_{max}	0.006	0.006	unitless
θ_C/K_{AD}	Not Applicable	110	a.u.

[+] set from the literature value for K_{CD} = 18 nM[2] and K_{AD} being on the order of hundreds of nM (100-1000 nM)[7]. Bounds were set from 0.018 to 0.18 to reflect this range.

3. Hill coefficient of the pexsD promoter

The pexsD promoter has been reported to be noncooperative (Hill coefficient n_{pexsD} ~1)[6]. To confirm that the Hill coefficient of the pexsD promoter is one, we placed ExsA under control of the pBAD promoter (pBAD-*exsA*) with the pexsD promoter driving GFP output (pexsD-*gfp*). We induced the pBAD promoter with arabinose and measured the output from the circuit (Fig. S2). Because there is no ExsD, we would expect the response (Fig. S2c) to be

$$output = F_{max}\frac{(A_0)^{n_{pexsD}}}{(A_0)^{n_{pexsD}} + K_{D,pexsD}^{n_{pexsD}}} + F_{min}\,, \tag{20}$$

where A_0 is derived from the promoter activity of the pBAD promoter (Equation 16, Table S1), $K_{D,\ pexsD}$ is the half-maximal concentration of the pexsD promoter, and F_{max} and F_{min} are the maximal and the basal expression of the pexsD promoter, respectively.

4. Characterizing the ultrasensitivity of the two-member system (Fig. 2)

The output of the two-member system can be described by the Hill-type equation[5]

$$output = F_{max}\frac{{A_0}^{n_H}}{{A_0}^{n_H} + K_H^{n_H}} + F_{min}\,, \tag{21}$$

where n_H is the apparent Hill coefficient and K_H is the apparent half-maximal concentration. Because the experiment was performed in an *E. coli* DIAL strain[8] and the characterized transfer functions were determined in *E. coli* DH10B (Table S1), the pBAD and pTet* promoters were

modeled again using Equation 16. All output data (at individual aTc concentrations) were fit simultaneously to the model (Equations 16 and 21) using fmincon in MATLAB 2014b (Fig. 2b). Table S3 shows the parameters.

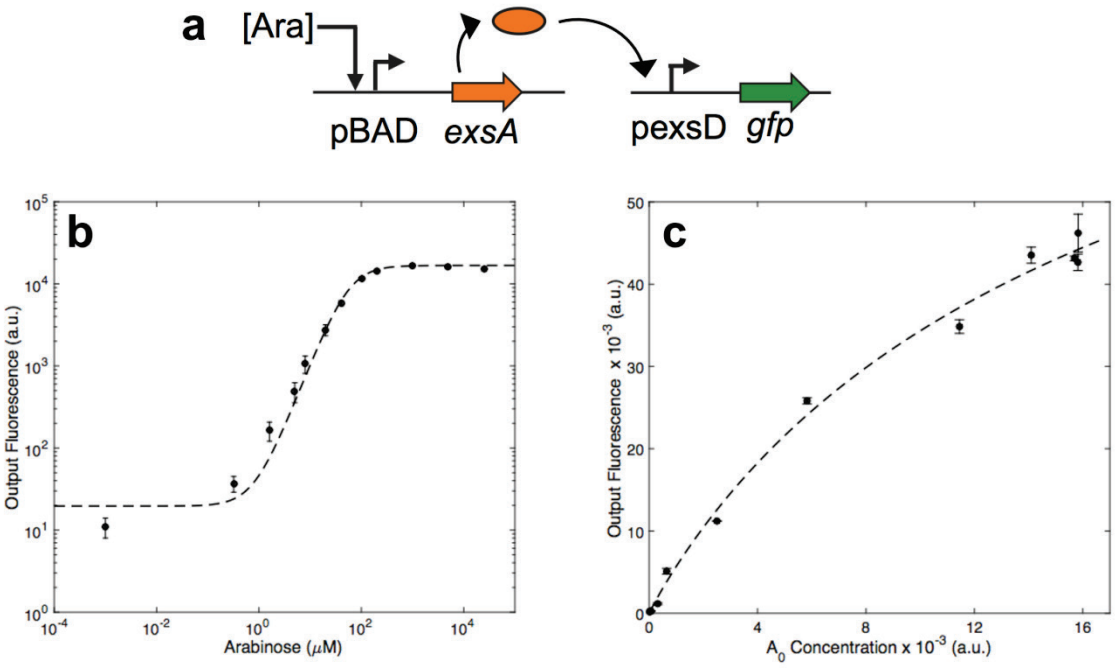

Figure S2. Transfer function of the pexsD promoter. a. Schematic diagram of a circuit constructed to characterize the pexsD promoter activity. **b**. Transfer function of the pBAD promoter. The dashed line represents a least squares regression fit using Equation 16 ($R^2 > 0.99$, Table S1). The pBAD promoter output was used to describe the A_0 concentration in arbitrary fluorescence units (a.u.). **c**. ExsA non-cooperatively activates the pexsD promoter. The dashed line shows a least squares regression fit using Equation 20 ($R^2 > 0.99$). The fitted parameters are: $n_{pexsD} = 0.95$, $K_{D,pExsD} = 1.8 \times 10^4$ a.u., $F_{min} = -32$, and $F_{max} = 9.4 \times 10^4$ a.u. The experimental data (solid circles) and error bars represent the averages and s.e.m of six replicates performed on three different days, respectively.

Table S3. Ultrasensitivity model parameters (Fig. 2). The ± values represent the 95% CI.

aTc (pg/mL)	D_0 (a.u.)	F_{max}	n_H	K_H	F_{min}/F_{max}
40	0.001	1.00 ± 0.01	1.0 ± 0.01	0.10 ± 0.01	$1.6 \times 10^{-3} \pm 1.0 \times 10^{-3}$
5.0×10^4	0.004	0.99 ± 0.01	1.1 ± 0.01	0.11 ± 0.01	$9.0 \times 10^{-5} \pm 3.3 \times 10^{-3}$
2.5×10^5	0.085	0.90 ± 0.03	2.3 ± 0.3	0.19 ± 0.01	$8.4 \times 10^{-3} \pm 1.1 \times 10^{-2}$
3.5×10^5	0.16	0.88 ± 0.02	3.4 ± 0.3	0.29 ± 0.01	$6.9 \times 10^{-3} \pm 9.0 \times 10^{-3}$
4.0×10^5	0.21	0.87 ± 0.02	3.8 ± 0.3	0.33 ± 0.01	$6.9 \times 10^{-3} \pm 8.0 \times 10^{-3}$
5.0×10^5	0.30	0.86 ± 0.02	5.0 ± 0.4	0.43 ± 0.01	$1.5 \times 10^{-2} \pm 0.7 \times 10^{-2}$

5. Determining hysteretic region boundaries (Fig. 3d and 4c)

We derived a model to fit the experimental data shown in Fig. 3d and 4c. We considered the steady state values for GFP and ExsA to be

$$GFP = GFP_{min} + GFP_{max}\frac{A}{A + K_{D,pexsD}} \tag{22}$$

and

$$A_0 = A_{min} + A_{max}\frac{A}{A + K_{D,pexsD}}. \tag{23}$$

Since ExsA is under control of a positive feedback loop (pexsD promoter), at steady-state, A_0 can be considered to be either in a fully ON or fully OFF state (i.e., bistable). When the system is in the fully ON state, $A \gg K_{D,pexsD}$, and when the system is in the fully OFF state, $A \ll K_{D,pexsD}$. Therefore, in the ON state $GFP_{ON} = GFP_{min} + GFP_{max}$ and in the OFF state $GFP_{OFF} = GFP_{min} + GFP_{max}A/K_{D,pexsD}$.

The experimental data shown in Fig. 3d and 4c is the fluorescence average of all the cells in both the ON and OFF populations. The normalized experimental output can be expressed as

$$\sigma = \rho_{ON} + (1 - \rho_{ON})GFP'_{OFF}, \tag{24}$$

where σ is the normalized output, ρ_{ON} is the fraction of cells in the ON population, $1 - \rho_{ON}$ is the fraction of cells in the OFF population, and $GFP'_{OFF} = \frac{GFP_{OFF}}{GFP_{ON}}$.

We observed that the fraction of cells in the ON population decreases sharply at a certain concentration of aTc and that at high aTc concentrations, the fraction of cells in the ON population is negligible. From this observation, we can define the fraction of cells in the ON population using a phenomenological Hill-type function[9]

$$\rho_{ON} = \frac{K^n}{[aTc]^n + K^n}. \tag{25}$$

Substituting Equation 25 into Equation 24 yields a mathematical model for the normalized experimental output

$$\sigma = GFP'_{OFF} + (1 - GFP'_{OFF})\frac{K^n}{[aTc]^n + K^n}. \tag{26}$$

The experimental data were fitted to Equation 26 using fmincon in MATLAB 2014b that minimizes the logarithmic sum of the squared errors (Fig. 3d and 4c). At high 3OC6 concentrations (Fig. 3d) or in the case of the dual-positive feedback system (Fig. 4c), the fluorescence of the ON cells does not reach zero (as discussed in Fig. S4). For both cases, GFP'_{OFF} is considered to be the GFP ratio $\frac{GFP_{Lower\ ON}}{GFP_{Higher\ ON}}$ rather than $\frac{GFP_{OFF}}{GFP_{ON}}$.

6. Characterizing the width of the hysteretic region as a function of ExsC (Fig. 3c)

The three-member system with a single positive feedback loop was modeled to characterize the effect of ExsC on the width of the hysteretic region. To simplify the analysis, we assumed that the amount of unbound ExsC in the system is negligible in the presence of excess ExsD. This assumption is valid when the ExsA-ExsD dissociation constant (K_{AD}) is much larger than the ExsD-ExsC dissociation constant (K_{DC}). K_{AD} has not been experimentally measured, but based on its position in the ExsADC signaling cascade, K_{AD} is suggested to be in the hundreds of nanomolar range[7]. K_{DC} has been experimentally determined to be 18 nM[2]. In order to solve our simplified model for the nullcline of A_0, we consider two cases: $C_0 < D_0$ and $C_0 \geq D_0$.

Case 1: $C_0 < D_0$

The mass balance for A_0 remains the same as Equation 1, but the mass balance equations for D_0 and C_0 can be simplified by our assumption that the amount of unbound ExsC in the system is negligible in the presence of excess ExsD. From Equations 3 and 2,

$$C_0 = DC \tag{27}$$

and

$$D_0 = D + DA + C_0 \,. \tag{28}$$

The ODEs describing the total protein concentrations D_0 and C_0 remain the same as Equations 5 and 6, but the ODE describing A_0 (Equation 4) becomes

$$\frac{dA_0}{dt} = \alpha_A \beta_A pexsD - \gamma_A A_0 \,. \tag{29}$$

At steady state, we solve for A_0

$$A_0 = \frac{\alpha_A \beta_A}{\gamma_A} pexsD = \theta_A{}' pexsD \,. \tag{30}$$

From Equations 15 and 30, we next obtain

$$A_0 = \theta_A{}' \left(F_{max} \frac{A}{A + K_{D,pexsD}} + F_{min} \right). \tag{31}$$

From Equations 1, 12, and 28, we obtain

$$A = \frac{1}{2}\left[A_0 - (D_0 - C_0) - K_{AD} + \sqrt{(A_0 - (D_0 - C_0) - K_{AD})^2 + 4A_0 K_{AD}} \right]. \tag{32}$$

Substituting Equation 32 into Equation 31 and non-dimensionalizing by K_{AD}, we obtain

$$\widehat{A_0} = \omega_A + \zeta_A \frac{\widehat{A_0} - \left(\widehat{D_0} - \widehat{C_0}\right) - 1 + \sqrt{\left(\widehat{A_0} - \left(\widehat{D_0} - \widehat{C_0}\right) - 1\right)^2 + 4\widehat{A_0}}}{\kappa + \widehat{A_0} - \left(\widehat{D_0} - \widehat{C_0}\right) - 1 + \sqrt{\left(\widehat{A_0} - \left(\widehat{D_0} - \widehat{C_0}\right) - 1\right)^2 + 4\widehat{A_0}}}, \quad (33)$$

where $\widehat{A_0} = \frac{A_0}{K_{AD}}$, $\widehat{D_0} = \frac{D_0}{K_{AD}}$, $\widehat{C_0} = \frac{C_0}{K_{AD}}$, $\omega_A = \frac{F_{min}\theta_{A'}}{K_{AD}}$, $\zeta_A = \frac{F_{max}\theta_{A'}}{K_{AD}}$, and $\kappa = \frac{2K_{D,pexsD}}{K_{AD}}$.

Case 2: $C_0 \geq D_0$

In this case, the amount of unbound ExsD is negligible due to excess ExsC. As a result, we expect $A=A_0$, leading to

$$A_0 = \theta_A{}' \left(F_{max} \frac{A_0}{A_0 + K_{D,pexsD}} + F_{min} \right). \quad (34)$$

Non-dimensionalizing Equation 34 by K_{AD} and solving for $\widehat{A_0}$, we obtain

$$\widehat{A_0} = \frac{1}{2}\left[\zeta_A + \omega_A - \frac{1}{2}\kappa + \sqrt{\left(\zeta_A + \omega_A - \frac{1}{2}\kappa\right)^2 + 2\omega_A\kappa} \right], \quad (35)$$

where $\omega_A = \frac{F_{min}\theta_{A'}}{K_{AD}}$, $\zeta_A = \frac{F_{max}\theta_{A'}}{K_{AD}}$, and $\kappa = \frac{2K_{D,pexsD}}{K_{AD}}$.

In addition to solving for the nullcline of A_0, we are also interested in the steady-state values D_0 and C_0. From Equations 9 and 10, we obtain

$$\widehat{D_0} = \omega_D + \zeta_D \frac{[aTc]^{n_{pTet*}}}{K_{D,pTet*}^{n_{pTet*}} + [aTc]^{n_{pTet*}}} \quad (36)$$

and

$$\widehat{C_0} = \omega_C + \zeta_C \frac{[3OC6]^{n_{pLux*}}}{K_{D,pLux*}^{n_{pLux*}} + [3OC6]^{n_{pLux*}}}, \quad (37)$$

where $\omega_D = \frac{F_{min}\theta_{D'}}{K_{AD}}$, $\zeta_D = \frac{F_{max}\theta_{D'}}{K_{AD}}$, $\omega_C = \frac{F_{min}\theta_{C'}}{K_{AD}}$ and $\zeta_C = \frac{F_{max}\theta_{C'}}{K_{AD}}$.

Using Equations 27-37, we investigated the effect of the ExsC concentration on the hysteretic region width, which is summarized in Fig. S3 and S4 as well as Fig. 3c.

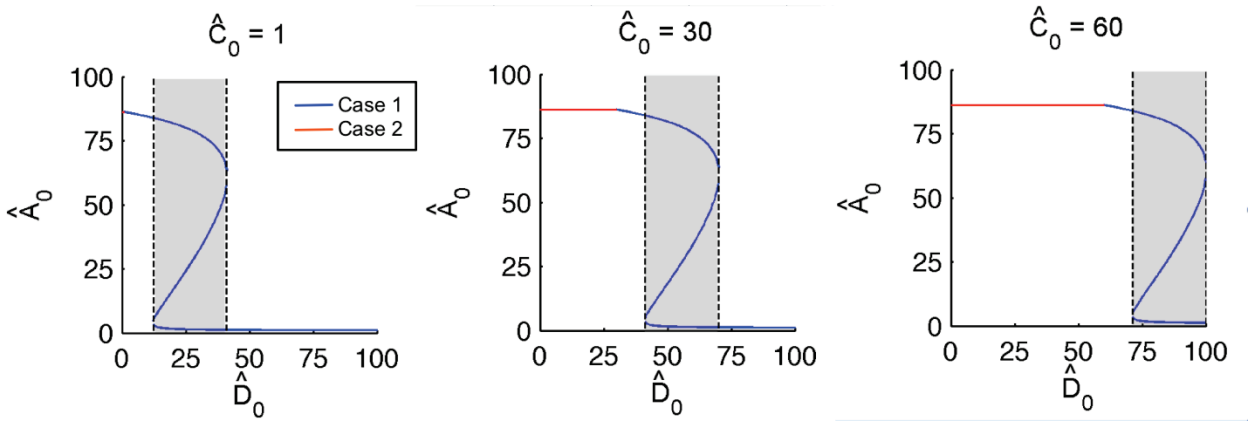

Figure S3. Nullcline shift with different concentrations of ExsC (Fig. 3c). The $\widehat{A_0}$ nullcline was plotted for three values of $\widehat{C_0}$. Both Case 1 and Case 2 were simulated, with Case 1 shown in blue and Case 2 in red. Increasing $\widehat{C_0}$ causes the nullcline to shift to the right while the shape of the nullcline does not change. The dashed black lines and gray boxes show the bistable region. The width of the bistable region in units of $\widehat{D_0}$ remains constant, independent of $\widehat{C_0}$. $\omega_A = 1$, $\zeta_A = 100$, and $\kappa = 30$.

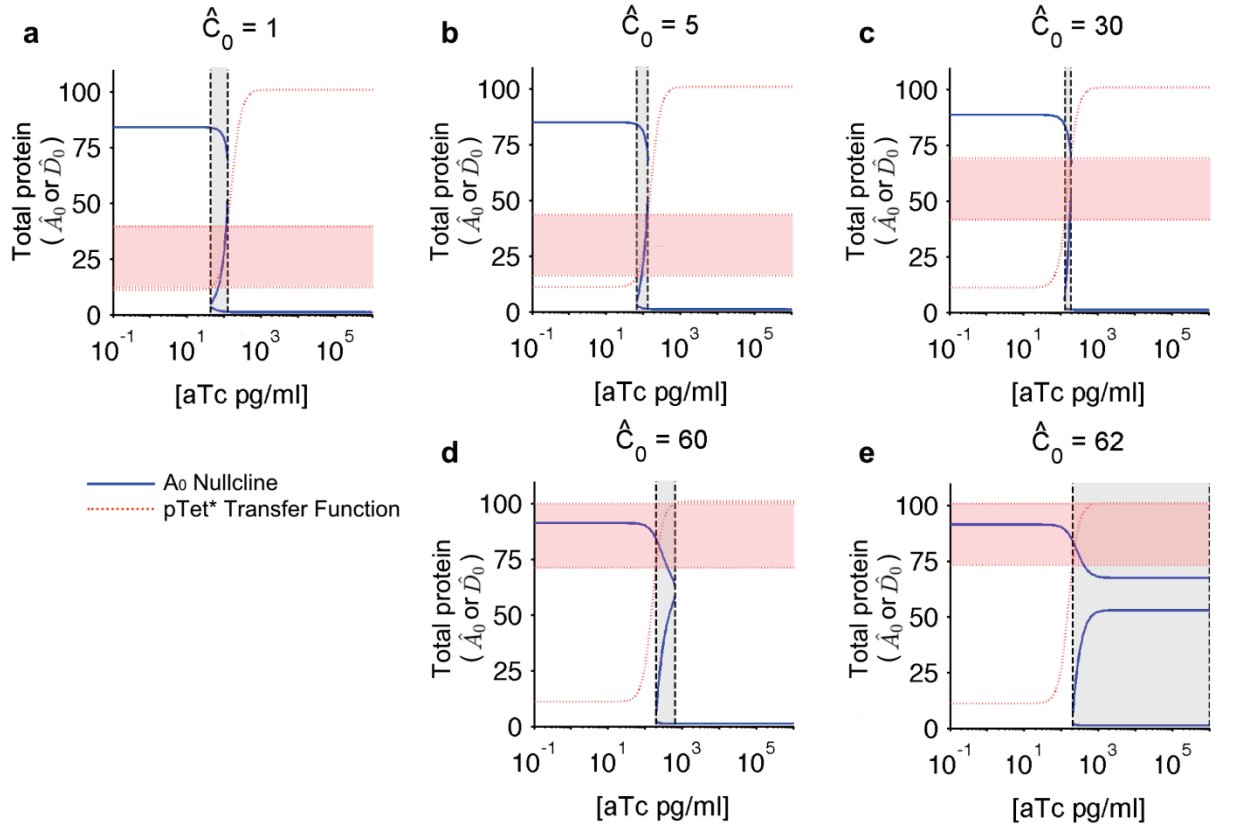

Figure S4. Effect of the inducible promoter controlling ExsD production on the hysteretic region width (Fig. 3c). Although the width of the bistable region remains constant with respect to $\widehat{D_0}$ (Fig. S3), the width of the bistable region in units of [aTc] appears to shrink and grow. The transfer function for pTet* driving production of $\widehat{D_0}$ (dotted red curve) is plotted in addition to the nullclines of $\widehat{D_0}$ (e.g., vertical dashed black lines) to illustrate this phenomenon. Note that the

x-axis is in units of [aTc] instead of $\widehat{D_0}$. The vertical dashed black lines and gray boxes highlight the hysteretic region in units of [aTc]. The horizontal dotted red lines and red boxes highlight the hysteretic region in units of $\widehat{D_0}$. The red box corresponds directly to the bistable region (gray box) from Fig. S3. While the bistable region shifts to higher $\widehat{D_0}$ regions linearly with additional $\widehat{C_0}$ in Fig. S3, the transfer function for $\widehat{D_0}$ is sigmoidal, leading to shrinking and stretching of the bistable region. As $\widehat{C_0}$ increases from Panel **a** to **c**, we observe a shrinking in the width of the bistable region, which is due to the steepness of the pTet* transfer function at this aTc range. As $\widehat{C_0}$ continues to increase from Panel **c** to **e**, the pTet* transfer function nears saturation at high concentrations of aTc, resulting in the increased hysteretic width. Once the pTet* promoter is completely saturated, the bistable region expands without bound since the upper limit of the hysteretic region is beyond the limit of the transfer function. In addition, the shape of the top $\widehat{A_0}$ nullcline (ON state) in Fig. S4e explains the lower ON states at the high 3OC6 (3.0 and 4.0 nM) and aTc (>1,000 pg/ml) concentrations in Fig. 3d. $\omega_A = 1, \zeta_A = 100, \kappa = 30, K_{D,pTet*} = 160, \omega_D = 11, \zeta_D = 90, n_{pTet*} = 3.3$.

7. Bifurcation diagram of the single- and dual-positive feedback systems (Fig. 4b)

We analyzed circuits with either one positive or two positive feedback loops to understand the effect of the feedback topology on the width of the bistable region. To simplify the analysis, we combined the equations for the change in D_0 and C_0 over time into that of a single variable M_0 (D_0 - C_0), describing the "effective" D_0 concentration.

For the dual-positive feedback system, ExsC is produced from the pexsD promoter, which changes Equation 6 to

$$\frac{dC_0}{dt} = \alpha_C \beta_C pexsD - \gamma_C C_0 \,. \tag{38}$$

Equation 38 was subtracted from Equation 5 to obtain the single equation

$$\frac{d}{dt}(D_0 - C_0) = (\alpha_D \beta_D pTet^* - \alpha_C \beta_C pexsD) - \gamma(D_0 - C_0) \,. \tag{39}$$

or

$$\frac{dM_0}{dt} = (\alpha_D \beta_D pTet^* - \alpha_C \beta_C pexsD) - \gamma M_0 \,. \tag{40}$$

Here we assumed $\gamma_D = \gamma_C = \gamma$ to simplify the analysis. The two non-dimensionalized equations for the dual-positive feedback system are

$$\frac{d\widehat{A_0}}{d\tilde{t}} = \omega_A + \zeta_A \left(\frac{\widehat{A_0} - \widehat{M_0} - 1 + \sqrt{\left(\widehat{A_0} - \widehat{M_0} - 1\right)^2 + 4\widehat{A_0}}}{\kappa + \widehat{A_0} - \widehat{M_0} - 1 + \sqrt{\left(\widehat{A_0} - \widehat{M_0} - 1\right)^2 + 4\widehat{A_0}}} \right) - \widehat{A_0} \tag{41}$$

and

$$\frac{d\widehat{M_0}}{d\tilde{t}} = \delta_M - \zeta_C \left(\frac{\widehat{A_0} - \widehat{M_0} - 1 + \sqrt{\left(\widehat{A_0} - \widehat{M_0} - 1\right)^2 + 4\widehat{A_0}}}{\kappa + \widehat{A_0} - \widehat{M_0} - 1 + \sqrt{\left(\widehat{A_0} - \widehat{M_0} - 1\right)^2 + 4\widehat{A_0}}} \right) - \widehat{M_0}\,, \qquad (42)$$

where $\tilde{t} = \gamma t$ and $\delta_M = \frac{\theta_D{}' pTet* - \theta_C{}' F_{min}}{K_{AD}}$. For the single positive feedback system, there is no ExsC, meaning $\theta_C{}' = 0$ and $\zeta_C = 0$.

To obtain bifurcation diagrams (Fig. 4b), each system was analyzed by setting Equations 41 and 42 equal to zero and solving for $\widehat{A_0}$ and $\widehat{M_0}$ simultaneously using MATLAB 2014b. The stability of each steady state was analyzed by numerically determining the trace and determinant value. As shown in Fig. S5, the nullclines of the single- and dual-positive feedback systems illustrate the difference in the bistable region width. Values for non-dimensionalized parameters were set to reasonable ranges based on the fitting values (Table S1 and S2) and are shown in Table S4.

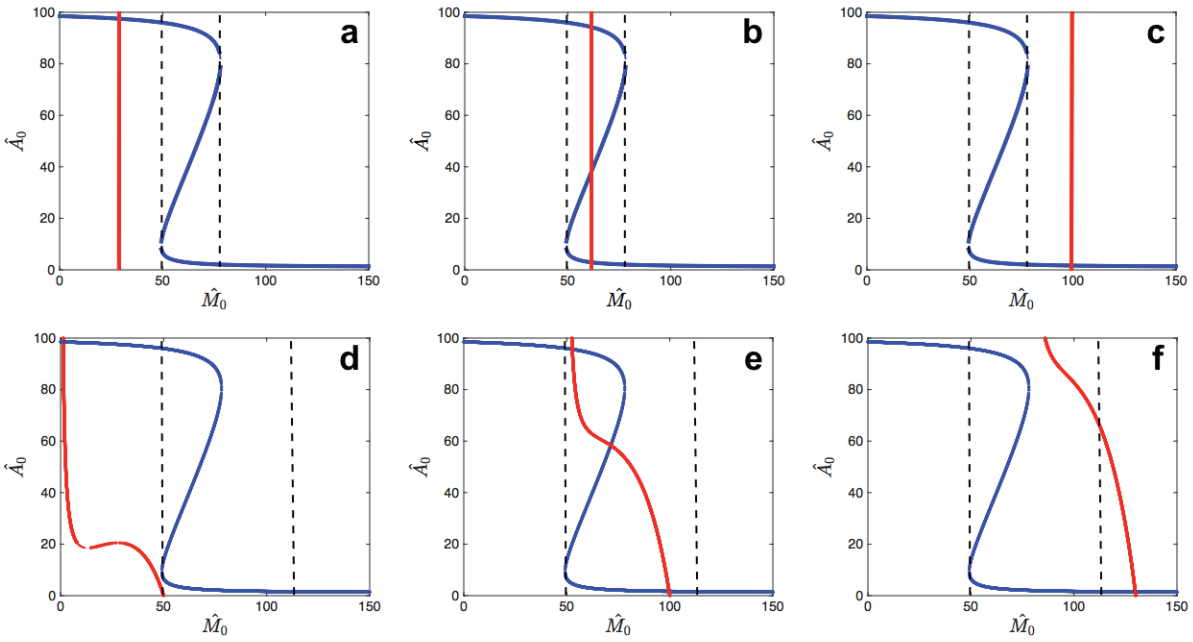

Figure S5. Nullclines of the single- and dual-positive feedback systems illustrating the difference in the bistable region width (Fig 4b). a-c. $\widehat{A_0}$ and $\widehat{M_0}$ nullclines for the single-positive feedback system. **d-f**. $\widehat{A_0}$ and $\widehat{M_0}$ nullclines for the dual-positive feedback system. **a,d.** Monostable ON. **b,e.** Bistable (with one unstable point in the middle). **c,f.** Monostable OFF. Bistable regions are between the black dashed lines and larger for the dual-positive feedback system than for the single-positive feedback system. Blue curve, $\widehat{A_0}$ nullcline; red curve/line, $\widehat{M_0}$ nullcline. κ = 5, ω_A= 1, and ζ_A= 100. For a-c, δ_M = 30, 60, and 100 from left to right; ζ_C= 0. For d-f, δ_M = 50, 100, and 130 from left to right; ζ_C= 50.

Table S4. Values used in the bifurcation diagrams (Fig. 4b). SPFB = single positive feedback; DPFB = dual positive feedback; δ_H and $pLux*$ for Section 8.

Variable	Definition	SPFB	DPFB	Justification
ζ_A	$\frac{F_{max}\theta_A{}'}{K_{AD}}$	30 - 130	30 - 130	Order of magnitude estimate, Table S2
ω_A	$\frac{F_{min}\theta_A{}'}{K_{AD}}$	1	1	Order of magnitude estimate, Table S2
ζ_C	$\frac{F_{max}\theta_C{}'}{K_{AD}}$	0	50	Order of magnitude estimate, Table S2
δ_M	$\frac{\theta_D{}'pTet^* - \theta_C{}'F_{min}}{K_{AD}}$	30 - 130	30 - 130	Order of magnitude estimate, Table S2
δ_H	$\frac{\theta_D{}'pTet^* - \theta_C{}'pLux^*}{K_{AD}}$	30 - 130	30 - 130	Order of magnitude estimate, Table S2
κ	$\frac{2K_{D,pexsD}}{K_{AD}}$	5	5	Fitted value for κ, Table S2
$pTet^*$	-	0 - 1	0 - 1	Promoter activity normalized to maximum fluorescence
$pLux^*$	-	0 - 1	0 - 1	Promoter activity normalized to maximum fluorescence

8. Bifurcation diagram of the tunable memory circuit (Fig. 3)

The circuit in Fig. 3 uses pLux* to control the amount of ExsC in the system. For this case, Equation 40 can be modified to

$$\frac{dM_0}{dt} = (\alpha_D\beta_D pTet* - \alpha_C\beta_C pLux*) - \gamma M_0. \tag{43}$$

The final non-dimensionalized equations are

$$\frac{d\widehat{A_0}}{d\tilde{t}} = \omega_A + \zeta_A\left(\frac{\widehat{A_0} - \widehat{M_0} - 1 + \sqrt{\left(\widehat{A_0} - \widehat{M_0} - 1\right)^2 + 4\widehat{A_0}}}{\kappa + \widehat{A_0} - \widehat{M_0} - 1 + \sqrt{\left(\widehat{A_0} - \widehat{M_0} - 1\right)^2 + 4\widehat{A_0}}}\right) - \widehat{A_0} \tag{44}$$

and

$$\frac{d\widehat{M_0}}{d\tilde{t}} = \delta_H - \widehat{M_0}\,, \tag{45}$$

where $\delta_H = \frac{\theta_D{}'pTet* - \theta_C{}'pLux*}{K_{AD}}$. Because the range of δ_H is similar to that of δ_M in Section 7 (Fig 4b, the single-positive feedback case) and Equations 44-45 are same as Equations 41-42 (with $\theta_C{}' = 0$ and $\zeta_C = 0$), the bifurcation diagram is identical.

9. Constructing different circuits with diverse topologies

The three-member, sequestration-based system is versatile in that it can be easily rewired to generate diverse topologies of interactions that enable different functions (Supplementary Fig. S6). The system provides flexible genetic parts that can be easily rearranged to generate diverse circuit behaviors (e.g., by adding the second *exsD*, from no feedback to negative feedback; or positive to coupled negative-positive feedback).

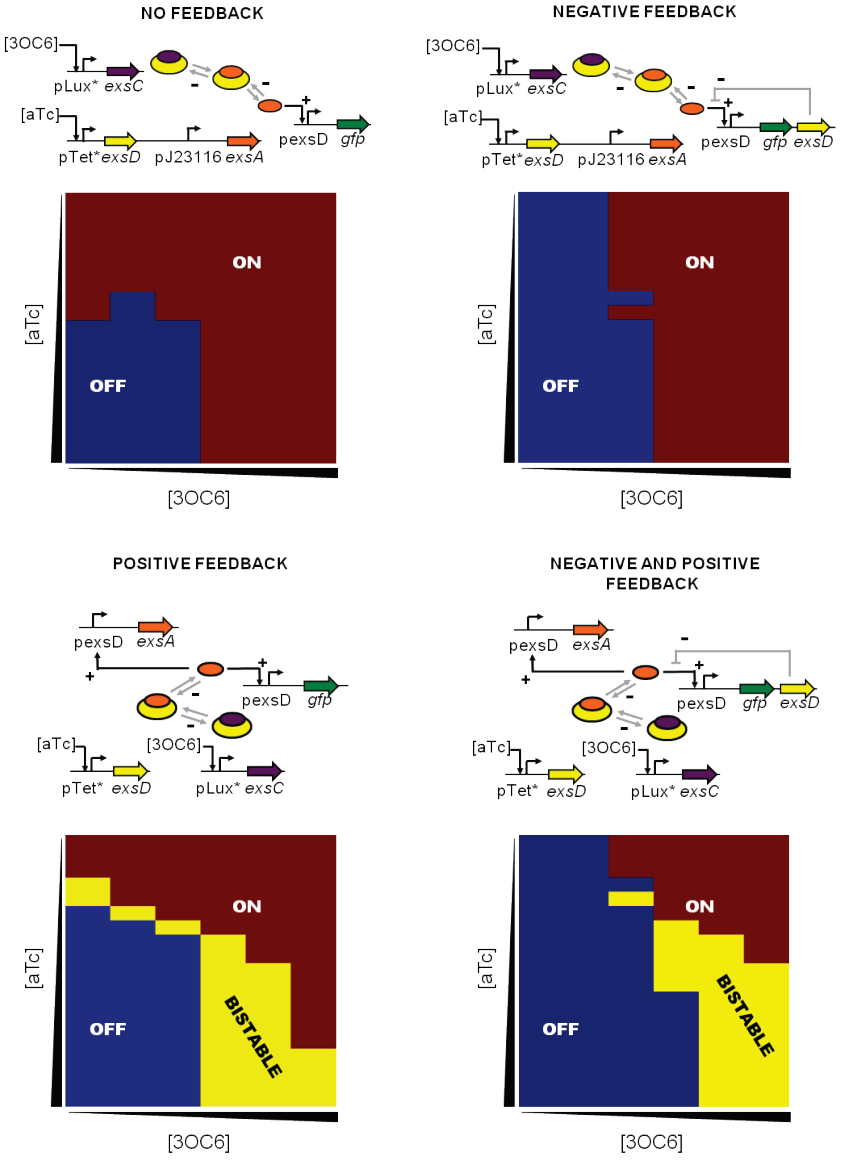

Figure S6. Diverse topologies of interactions obtained by rearranging the regulators (ExsADC). Bifurcation diagrams were generated by clustering flow cytometry data into BISTABLE (yellow), monostable ON (burgundy), and OFF (dark blue) using an EM algorithm with a GMM model as described in the Methods section. The experiments were performed at aTc concentrations of 0, 0.128, 0.64, 3.2, 5, 8, 16, 25, 30, 40, 50, 80, 100, 400, 2,000, 10,000, 50,000, 100,000, 250,000, and 500,000 pg/ml (from top to bottom) and 3OC6 concentrations of 0, 0.32, 1.6, 5, 8, and 15 nM (from left to right). pJ23116, constitutive promoter (Table S7). +, activating interaction; -, repressing interaction.

Table S5. List of plasmids used in this study.

Plasmid Name	Origin	Resistance	Properties
pTS001	p15A	AmpR	pBAD-*exsA*
pTS005	ColE1	CmR	pexsD-*gfp*
pTS023	p15A	AmpR	pexsD-*exsA*
pTS057	p15A	AmpR	pTet*-*exsD*-pBAD-*exsA*
pTS118	pSC101*	KanR	pexsD-*gfp*
pTS120	pSC101*	KanR	pexsD-*gfp*-*exsD*
pTS122	pSC101*	KanR	pLux*-*exsC*
pTS172	p15A	AmpR	pexsD-*exsA*-pLux*-*exsC*
pTS176	ColE1	CmR	pTet*-*gfp*
pTS177	p15A	AmpR	pexsD-*exsAC*
pTS186	R6K	KanR	pTet*-*exsD*
pTS206	ColE1	CmR	BBa_J23116-*exsA*-pTet*-*exsD*
pTS215	p15A	AmpR	pLux*-*gfp*
pTS219	P15A	AmpR	pBAD-*gfp*
pTS225	ColE1	CmR	pTet*-*exsD*
pTM007	p15A	AmpR	pLux*-*exsC*

Table S6. List of strains used in this study.

Name	Host Strain	Plasmids	Figure
TS064	DH10B	pTS057 + pTS005	Fig. 1b
TS141	DH10B	pTS057 + pTS005 + pTS122	Fig. 1c
TS188	JTK164A	pTS001 + pTS005 + pTS186	Fig. 2
TS198	DH10B	pTS172 + pTS118 + pTS225	Fig. 3 & Fig. S6
TS168	DH10B	pTS023 + pTS118 + pTS225	Fig. 4 (left)
TS167	DH10B	pTS177 + pTS118 + pTS225	Fig. 4 (right)
TS035	DH10B	pTS001 + pTS005	Fig. S2
TS210	DH10B	pTS206 + pTM007 + pTS118	Fig. S6
TS214	DH10B	pTS206 + pTM007 + pTS120	Fig. S6
TS202	DH10B	pTS172 + pTS120 + pTS225	Fig. S6

Table S7. List of genetic parts used in this study.

Part Name	Type and Source	DNA sequence
exsA	Gene[10]	atgcaaggagccaaatctcttggccgaaagcagataacgtcttgtcattggaacattccaactttcgaatacagggtaaacaa ggaagagggcgtatatgttctgctcgagggcgaactgaccgtccaggacatcgattccacttttgcctggcgcctggcgag ttgcttttcgtccgccgcggaagctatgtcgtaagtaccaagggaaaggacagccgaatactctggattccattatctgccca gtttctacaaggcttcgtccagcgcttcggcgcgctgttgagtgaagtcgagcgttgcgacgagcccgtgccgggcatcatc gcgttcgctgccacgcctctgctggccggttgcgtcaaggggttgaaggaattgcttgtgcatgagcatccgccgatgctcg cctgcctgaagatcgaggagttgctgatgctcttcgcgttcagtccgcaggggccgctgctgatgtcggtcctgcggcaact gagcaaccggcatgtcgagcgtctgcagctattcatggagaagcactacctcaacgagtggaagctgtccgacttctcccg cgagttcggcatggggctgaccaccttcaaggagctgttcggcagtgtctatggggtttcgccgcgcgcctggatcagcga gcggagaatcctctatgcccatcagttgctgctcaacagcgacatgagcatcgtcgacatcgccatggaggcgggcttttcc agtcagtcctatttcacccagagctatcgccgccgtttcggctgcacgccgagccgctcgcggcaggggaaggacgaatg ccgggctaaaaataactga
exsD	Gene[10]	atggagcaggaagacgataagcagtactcccgagaagcggtgttcgctggcaggcgggtatccgtggtgggctcggacg cccgctcgcggggtcgggtgccgggttacgcatcgagcagtttgtatcgtgagtccggaatcatcagtgcgcggcaactg gcgttgctgcagcggatgctgccgcgcctgcggctggagcaactgttccgctgcgagtggttgcagcagcgcctggcgc gcggcctggcgctggggcgcgaagaggtgcggcagattctcctctgcgcggcgcaggacgacgacggctggtgctccg aactgggcgaccgggtcaacctcgccgtgccgcagtcgatgatcgactgggtcctgctgccggtctatggctggtgggaa agcctgctcgaccaggcgatcccggctggcgcctgtcgctggtggagctggagacccagtcccggcaactgcgagtca agtccgaattctggtcccgcgtggccgagctggagccggagcaggcccgcgaggaactggccagggtcgccaagtgcc aggcgcgcacccaggaacaggtggccgaactggccggcaagctggagacggcttcggcactggcgaagagcgcctgg ccgaactggcagcggggcatggcgacgctgctcgccagcggcgggctggccggcttcgagccgatccccgaggtcctc gaatgcctctggcaacctctctgccggctggacgacgacgtcggcgcggcggacgccgtccaggcctggctgcacgaac gcaacctgtgccaggcacaggatcacttctactggcagagctga
exsC	Gene[10]	atggatttaacgagcaaggtcaaccgactgcttgccgagttcgcaggccgtatcggtttgccttccctgtccctcgacgagg agggcatggcgagcctcctgttcgacgaacaggtgggcgtcaccctgttgctgctcgccgagcgcgagcgtctgttgctg gaggccgatgtggcgggcatcgatgtgctgggcgaggggatctttcgccagctcgccagcttcaaccgccattggcaccg tttcgatctgcatttcggcttcgacgagctgaccggcaaggtccagttgtatgcgcagattctcgcagcgcaactgaccctcg aatgcttcgaggcgaccttggccaatctgctcgatcacgccgagttctggcagcgcctgctgccgtgcgacagtgatcgcg aggcggtcgctgcggtcggcatgagggtttga
gfp	Gene[11]	atgagtaaaggagaagaacttttcactggagttgtcccaattcttgttgaattagatggtgatgttaatgggcacaaatttttctgt cagtggagagggtgaaggtgatgcaacatacggaaaacttacccttaaatttatttgcactactggaaaactacctgttccatg gccaacacttgtcactactttgacttatggtgttcaatgcttttcaagatacccagatcatatgaaacggcatgactttttcaaga gtgccatgcccgaaggttatgtacaggaaagaactatatttttcaaagatgacgggaactataagacacgtgctgaagtcaa gtttgaaggtgatacacttgttaatagaatcgagttaaaaggtattgattttaaagaagatggaaacattcttggacacaagttg gaatacaactataactcacacaatgtatacatcatggcagacaaacaaaagaatggaatcaaagttaacttcaaaattagaca caacattgaagatggaagcgttcaactagcagaccattatcaacaaaatactccaattggcgatggccctgtccttttaccag acaaccattacctgtccacacaatctgccctttcgaaagatcccaacgaaaagagagaccacatggtccttcttgagtttgtaa cagctgctgggattacacatggcatggatgaactatacaaaaggcctgcagcaaacgacgaaaactacgcttaa
pexsD	Promoter[10]	gaaggacgaatgccgggctaaaaataactgacgtttttgaaagcccggtagcggctgcatgagtagaatcggcccaaat
pTet*	Promoter[3]	ttttcagcaggacgcactgacctccctatcagtgatagagattgacatccctatcagtgatagagatactgagcacatat
pLux*	Promoter[3]	acctgtaggatcgtacaggtttacgcaagaaaatggtttgttactttcgaataaa
pBAD	Promoter[11]	agaaaccaattgtccatattgcatcagacattgccgtcactgcgtcttttactggctcttctcgctaaccaaaccggtaaccccg cttattaaaagcattctgtaacaaagcgggaccaaagccatgacaaaaacgcgtaacaaaagtgtctataatcacggcagaa aagtccacattgattatttgcacggcgtcacactttgctatgccatagcatttttatccataagattagcggatcctacctg
BBa_J23116	Promoter (http://parts.igem.org/Promoters/Catalog/Anderson)	ttgacagctagctcagtcctagggactatgctagc

References

1 Thibault, J., Faudry, E., Ebel, C., Attree, I. & Elsen, S. Anti-activator ExsD forms a 1:1 complex with ExsA to inhibit transcription of type III secretion operons. *The Journal of biological chemistry* **284**, 15762-15770 (2009).

2 Lykken, G. L., Chen, G., Brutinel, E. D., Chen, L. & Yahr, T. L. Characterization of ExsC and ExsD self-association and heterocomplex formation. *Journal of Bacteriology* **188**, 6832-6840 (2006).

3 Moon, T. S., Lou, C. B., Tamsir, A., Stanton, B. C. & Voigt, C. A. Genetic programs constructed from layered logic gates in single cells. *Nature* **491**, 249-253 (2012).

4 Ferrell, J. E., Jr. Tripping the switch fantastic: how a protein kinase cascade can convert graded inputs into switch-like outputs. *Trends in Biochemical Sciences* **21**, 460-466 (1996).

5 Buchler, N. E. & Cross, F. R. Protein sequestration generates a flexible ultrasensitive response in a genetic network. *Molecular Systems Biology* **5**, 272-272 (2009).

6 Brutinel, E. D., Vakulskas, C. A., Brady, K. M. & Yahr, T. L. Characterization of ExsA and of ExsA-dependent promoters required for expression of the Pseudomonas aeruginosa type III secretion system. *Mol Microbiol* **68**, 657-671 (2008).

7 Bernhards, R. C., Marsden, A. E., Esher, S. K., Yahr, T. L. & Schubot, F. D. Self-trimerization of ExsD limits inhibition of the Pseudomonas aeruginosa transcriptional activator ExsA in vitro. *FEBS Journal* **280**, 1084-1094 (2013).

8 Kittleson, J. T., Cheung, S. & Anderson, J. C. Rapid optimization of gene dosage in E. coli using DIAL strains. *Journal of biological engineering* **5**, 10 (2011).

9 Nevozhay, D., Adams, R. M., Van Itallie, E., Bennett, M. R. & Balazsi, G. Mapping the Environmental Fitness Landscape of a Synthetic Gene Circuit. *Plos Comput Biol* **8**, e1002480 (2012).

10 Stover, C. K. *et al.* Complete genome sequence of Pseudomonas aeruginosa PAO1, an opportunistic pathogen. *Nature* **406**, 959-964 (2000).

11 Temme, K. *et al.* Induction and relaxation dynamics of the regulatory network controlling the type III secretion system encoded within Salmonella Pathogenicity Island 1. *Journal of Molecular Biology* **377**, 47-61 (2008).